Original Article

Degradation-induced Changes of Mechanical Properties of an Electro-spun Polyester-urethane Scaffold for Soft Tissue Regeneration

Hugo Krynauw, Lucie Bruchmüller[#], Deon Bezuidenhout, Peter Zilla, Thomas Franz*

Cardiovascular Research Unit, Chris Barnard Department of Cardiothoracic Surgery, Faculty of Health Sciences, University of Cape Town, Private Bag X3, Observatory 7935, South Africa

Running head: Degradation-induced Mechanics of Scaffold for Tissue Regeneration

* Corresponding author:
Thomas Franz, PhD
Cardiovascular Research Unit
Faculty of Health Sciences
University of Cape Town
Private Bag X3, Observatory 7935, South Africa
Tel.: +27 21 406 6410; Fax: +27 21 448 5935
Email: Thomas.Franz@uct.ac.za

Permanent address: Department of Chemical and Process Engineering, Karlsruhe Institute of Technology, Karlsruhe, Germany

Published in Journal of Biomedical Materials Research B.
Full reference: Krynauw H, Bruchmüller L, Bezuidenhout D, Zilla P, Franz T. Degradation-induced change in mechanical properties of an electro-spun polyester-urethane scaffold for vascular tissue regeneration. J Biomed Mater Res B, 2011, DOI: 10.1002/jbm.b.31907

ABSTRACT

The aim of this study was the *in vitro* investigation of the change in mechanical properties of a fast-degrading electro-spun polymeric scaffold for the use in soft tissue regenerative implants. Tubular scaffolds were electro-spun from a DegraPol® D30 polyesther-urethane solution (target outer diameter: 5.0 mm; scaffold wall thickness: 0.99±0.18 mm). Scaffold samples were subjected to hydrolytic *in vitro* degradation for up to 34 days. The fibre network structure and fibre surfaces were inspected on scanning electron micrographs. Following vacuum drying and determination of mass, flat samples (9.69±0.21 x 18.47±2.62 mm, n = 5) underwent uni-axial tensile testing (5 load cycles, strain ε = 0 to 20%; final extension to failure) in circumferential scaffold direction after 5, 10, 14, 18, 22, 26, 30 and 34 days of degradation. Scaffold mass did not change with degradation. Maximum elastic modulus, maximum stress and associated strain were E_{max} = 1.14±0.23 MPa, σ_{max} = 0.52±0.12 MPa and ε_{max}= 176.8±21.9% before degradation and E_{max} = 0.43±0.26 MPa, σ_{max} = 0.033±0.028 MPa and ε_{max} = 24.6±3.0% after 34 days of degradation. The deterioration of mechanical properties was not reflected in the ultrastructural surface morphology of the fibres. The current exploratory study provides a basis for the development of constitutive computational models of biodegradable scaffolds with future extension of the investigation most importantly to capture mechanical effects of regenerating tissue. Future studies will include degradation in biological fluids and assessment of molecular weight for an advanced understanding of the material changes during degradation.

Keywords: Electro-spinning, hydrolytic degradation, elastic modulus, material properties, DegraPol®, soft tissue regeneration

1. INTRODUCTION

Tissue engineering and tissue regeneration are prominent tools in regenerative medicine for the treatment of diseases and injuries.[1,2] Biodegradable scaffolds have been used and have shown promises for the future of tissue regenerative prosthesis. Implants need to be designed such that their behaviour matches, in the ideal case both biologically and mechanically, that of the organ or tissue to be replaced in its healthy state.[1] In tissue regenerative implants, porosity allowing the ingrowth of cells and tissue is a key factor for the long-term success.[3-5] Porous scaffolds have been manufactured in different ways including phase inversion and porogen extraction,[6,7] salt leaching,[8] gas foaming,[9] extrusion-phase-inversion,[10] thermally induced phase separation[11] and electro-spinning.[12-14]

While imperative for healing and tissue regeneration, porosity may adversely affect the mechanical properties of the scaffold, in particular when viscoelastic polymeric materials are used. This, together with the aim of providing implants that mimic complex physiological mechanics, increases the complexity of the design of tissue regenerative implants. Thus, computational methods have been employed for the development and optimization of implants.[15-18] These methods require the knowledge of the mechanical properties of the scaffold which are typically determined in experimental tests.[15,19]

For tissue regenerating implants, computational models need to account for the effects of the ingrowth of cells and tissue on the structural properties of the implant. In the case of biodegradable scaffold materials, the effect of the degradation process on mechanical and structural properties of the porous scaffolds is yet another aspect to be considered. Both tissue ingrowth and biodegradation are transient processes which change the mechanical and structural properties of the implanted device over time. The ingrowth of cells and tissue typically results in an increase in structural stiffness[20] whereas scaffold degradation, occurring concurrently with tissue ingrowth, leads to loss of mechanical properties and potentially to structural disintegration.

The optimal design of tissue regenerative prostheses, thus, needs to consider the mechanical properties of the initial scaffold as well as effects of healing and bio-degradation on the structural mechanics of the implant. Consequently, detailed knowledge is required of the mechanical effects of tissue regeneration and biodegradation.

The mechanical characterization of biodegradable polymeric materials used for tissue regenerative medical implants, has received attention from various research groups. Lendlein et al.[21,22] studied the mechanical bulk properties of a degradable polyester-urethane (DegraPol®) prior to degradation and during degradation, whereas electro-spun polyester-urethane membranes were mechanically characterised by Riboldi et al.[14] Kwon et al.[23] determined structural and mechanical properties of electro-spun biodegradable co-polyesters. Mechanical properties prior to degradation have also been reported for electro-spun scaffolds using poly(ε-caprolactone)[24], poly(ε-caprolactone)/collagen[25] and poly(ε-caprolactone)/poly-lactic acid.[26]

The change of mechanical properties associated with degradation has been studied for various biodegradable polymers. Raghunath et al.[27] characterised solid sheets of biodegradable polyhedral oligomeric silsesquioxane modified poly(caprolactone/carbonate) urethane/urea during accelerated *in vitro* degradation of up to eight weeks. Kang et al.[4] studied the *in vitro* degradation of a porous poly(l-lactic acid)/β-tricalcuim phosphate scaffold, fabricated by particulate leaching, of up to six weeks and reported the effect on the compressive strength.

While the mechanics of electro-spun degradable scaffolds has been investigated prior to degradation, the information on the effects of the degradation process on the mechanical properties is limited. Lee et al.[25] studied the maintenance of tensile properties of electro-spun poly(ε-caprolactone)/collagen scaffolds subjected to a perfusion bioreactor environment for up to four weeks. Henry et al.[28] mechanically characterised electro-spun meshes of a slow degrading polyester-urethane during hydrolytic *in vitro* degradation of up to 346 days.

In this study, we investigated electro-spun fast-degrading polyester-urethane scaffolds. The fibrous network of the scaffolds provides porosity required for cell and tissue ingrowth. This feature,

combined with the biodegradable nature of the polymer used, offers these scaffolds for potential application in soft tissue regenerative therapies. The change of structural and mechanical properties of the scaffold was studied during hydrolytic *in vitro* degradation of up to 34 days.

2. MATERIALS AND METHODS

2.1. Material

DegraPol® (ab medica S.p.A, Lainate, Italy) is a biodegradable polyester-urethane that consists of poly(3-(R- hydroxybutyrate)-co-(ε-caprolactone))-diol (hard segment) and poly(ε-caprolactone-co-glycolide)-diol (soft segment). Both polymer segments are biodegradable and their degradation products are non-toxic.[29] By using different ratios of hard and soft segment the mechanical properties of the final product can be modulated, whereas by changing the ratio of ε-caprolactone to glycolide the degradation characteristics can be modulated. This versatility, combined with the non-toxicity and haemocompatibility makes DegraPol® a promising choice for tissue engineering scaffolds. DegraPol® D30 has a ε-caprolactone-to-glycolide ratio of 70:30 and a hard-to-soft segment ratio of 40:60 (unpublished data). The electro-spinning solution was prepared by dissolving DegraPol® D30 in chloroform with a 20% by weight concentration at room temperature and subsequently sonicating in distilled water at 37°C for 90 min.

2.2. Electro-spinning and sample preparation

Eight tubular samples were prepared by electro-spinning the DegraPol® solution from a hypodermic needle with a flow rate 1.437 ml/h (SE400B syringe pump, Fresenius, Bad Homburg, Germany) onto a tubular target （hypodermic tubing, Small Parts, Loganport, IN, USA; outer diameter: 5.0 mm) rotating at 400 RPM and bi-directionally translating orthogonal to the needle, over a length of 95 mm at a speed of 2.6 mm/min (custom-made drive mechanism). The electrostatic field of 13 kV between the hypodermic needle and the target (distance: 200 mm) was produced by a custom-made high voltage supply. After completion of the spinning process, the electro-spun structure on the target hypotube was submersed in ethanol for 5 minutes, cut open lengthwise, removed from the mandrel and dried under vacuum (Townson & Mercer Ltd, Stretford, England; room temperature, 90min). Due

to the decreasing wall thickness in the end regions, 10 - 20 mm was cut off on either end of the electro-spun tube and discarded. The remaining part of the tubular sample was cut into 10mm wide strips yielding 10 × 18.5 mm rectangular samples (when unfolded) with the longer edge aligned with spinning rotational direction of the target.

2.3. *In vitro* hydrolytic degradation

For *in vitro* hydrolytic degradation, single samples were placed in a container with 2 ml distilled water and kept at 37°C (incubator, Scientific Engineering, Johannesburg, South Africa) for degradation time periods of T = 5, 10, 14, 18, 22, 26, 30 and 34 days (n = 5 samples at each time point). An additional time point of T = 0 days refers to non-degraded reference samples. Since the polymer is fast-degrading, non-degraded samples were not soaked, as this would have initiated degradation. After degradation, the samples were removed from water and dried in a vacuum (Townson & Mercer Ltd, Stretford, England; room temperature, 90 min). The pH of the degradation fluid of three samples was measured twice a week (Jenway pH meter 3320, Bibby Scientific Limited, Staffordshire, UK).

2.4. Physical characterisation

Physical characterisation included microscopic inspection of fibre diameter and alignment, measurement of mass and dimensions of the samples, determining scaffold porosity, and uni-axial tensile testing. Samples for scanning electron microscope (SEM) analysis were sputter coated with gold in a Polaron SC7640 (Quorum Technologies, East Grinstead, England). Images were taken of the internal, external and cut surfaces of the samples with a JEOL JSM5200 scanning electron microscope (JEOL Ltd, Tokyo, Japan) at 25 kV. Fibre diameter was measured with Scion Image for Windows (Scion Corporation, Frederick, USA) on x2000 SEM micrographs (one image per sample, ten measurements per image).

Wall thickness, width and length of scaffold samples were measured on images captured on a Leica DFC280 stereo microscope using Leica IM500 imaging software (Leica Microsystems GmbH, Wetzlar, Germany). Six thickness measurements were recorded on both length edges of each sample

as well as six measurements for sample width. The sample mass was determined using a Mettler Toledo XS105S analytical balance (Mettler Toledo, Greifensee, Switzerland).

Fibre alignment of non-degraded and degraded samples was computed by analysing two-dimensional Fast Fourier Transforms (2D FFT) of the ×200 SEM micrographs in ImageJ (National Institute of Health, Bethesda, MD, USA). All text and borders were cropped from the image prior to applying the 2D FFT. The FFT represents the frequency spectrum of the change in pixel intensity of an image. When fibres are aligned (Fig. 1a), the frequency of pixel intensity change will be greater orthogonal to the fibres than in line with them. By using the ImageJ Oval Profile Plot plug-in (written by William O'Connell), a radial summation of pixel intensity in a circular field on the FFT power spectrum (Fig. 1b) can be presented as the fibre alignment orthogonal to summation angle.[13,30,31] By scaling the summation results of all images to lie between 0 and 1, the difference in brightness, contrast and number of fibres per image can be normalised.

Scaffold porosity, P, formed by the fibrous network, was calculated from total volume V_T and fibre volume V_F of scaffold samples as $P = 1 - V_F/V_T$. The total volume, i.e. volume of fibres and pores, was determined from wall thickness, width and length of the samples (n = 3) measured as described above. The fibre volume, defined as the volume occupied by the fibres excluding all open spaces (pores), was determined by hydrostatic weighing typically employed for density determination. The dry samples were weighed a) in air and b) while submerged in ethanol, eliminating all air from the scaffold (Adam AAA250L analytical balance with Adam density determination kit, Adam Equipment Inc, Danbury, CT, USA). The difference in mass of the scaffold sample measured in air, $m_{S,air}$, and in ethanol, $m_{S,eth}$, caused by the buoyancy force exerted on the submerged scaffold, equals the mass of the ethanol, m_E, that is displaced by the fibres: $m_E = m_{S,air} – m_{S,eth}$. The volume of the displaced ethanol, V_E, was calculated from the mass, m_E, and the known density of ethanol, ρ_E, as $V_F = V_E = m_E / \rho_E$. Since the volume of the ethanol displaced by the fibres equals the volume of the fibres, the latter is obtained as $V_F = V_E$.

Tensile testing was performed on dry samples at room temperature on an Instron 5544 universal testing machine (Instron, Norwood, USA) using custom made clamps. The test protocol comprised five pre-cycles (0 to 20 % strain, 20 mm/min crosshead speed, data sampling at 0.1% strain intervals) and a final extension until complete failure (20 mm/min crosshead speed data sampling at 0.1% strain intervals).

2.5. Data analysis

The data recorded were maximum stress σ_{max} and the associated strain ε_{max}, the stress at the upper strain limit of $\varepsilon = 20\%$ of each load cycle, $\sigma_{20\%,i}$, where i denotes the number of the load cycle with i = 1 to 5, and the stress at $\varepsilon = 20\%$ of the final loading, $\sigma_{20\%,i}$, with i = 6. The change in stress associated with cycling was expressed as the ratio, $\sigma_{20\%,6} / \sigma_{20\%,1}$, of the stress at $\varepsilon = 20\%$ during the final and the first loading.

The elastic modulus was determined as the slope of the stress-strain curves for the first and the final loading at discrete strain values, $E_{\varepsilon,i}$, where ε refers to the strain value with $\varepsilon = 0$, 4, 8, 12, 16 and 18%, and i refers to the number of the loading with i = 1 and 6. After smoothing of the stress-strain data (moving average filter, half-width: 3), the slope was calculated for the strain range [$\varepsilon - 0.1\%$, $\varepsilon + 0.1\%$] and filtered (moving average filter, half-width: 5). This procedure resulted in elastic modulus values averaged over a range of [$\varepsilon - 0.9\%$, $\varepsilon + 0.9\%$] for each discrete value of strain of $\varepsilon = 0$, 4, 8, 12, 16 and 18%.

2.6. Comparative fibre alignment analysis

For comparison purposes, the 2D FFT method described in Section 2.5 was applied to a SEM micrograph published by Riboldi et al. (Fig.1a)[14] to determine the amount of fibre alignment of the electro-spun scaffold used in that study.

2.7. Statistical analysis

For quantitative data, one-way ANOVA was performed when more than two groups were compared by using Tukey HSD post-hoc analysis with $p < 0.05$ indicating statistical significance. Data are expressed as mean values ± standard deviation.

3. RESULTS

3.1. Dimensions and structure of electro-spun scaffolds

The average wall thickness of the tubular scaffolds was 0.99 ± 0.18 mm. The width and length of the samples for tensile testing was 9.69 ± 0.21 mm and 18.47 ± 2.62 mm, respectively. The tensile test gauge length was 10.40 ± 0.31 mm. Fibre diameter was 6.80 ± 2.96 μm, ranging between 1.73 μm and 16.45 μm.

Figure 2(a, b) shows the cross-section of the electro-spun scaffold at low magnification whereas Fig. 2(c-f) depict the fibrous structure at higher magnification. The fibre alignment of the inner and outer surface of the wall is illustrated Fig. 3. The graphs indicate predominant alignment of the fibres at an angle of 85 to 90° (the latter value representing the circumferential direction of the electro-spun tube) with a more pronounced alignment observed on the outer surface compared to the inner surface of the tube. There was no difference in fibre alignment between non-degraded and degraded samples.

The fibre surfaces of scaffold samples after 14 and 34 days degradation prior to mechanical testing are shown in Fig. 2(g, h). Figure 4(a,b) and (c,d) provide scanning electron micrographs of scaffold samples that were degraded for 5 and 26 days, respectively, after mechanical testing to failure.

The scaffold porosity was determined to be 80 ±2%.

3.2. pH of degradation fluid

The degradation fluid had an initial pH of 7.2±0.1. At T = 6 days the pH had dropped to 5.9 ± 0.2, after which it remained in this level, ending at 5.7 ± 0.4 at T = 34 days.

3.3. Mass loss of scaffold

The scaffold mass did not change significantly over the degradation period. Figure 5 shows the cumulative loss of mass as a percentage of the original sample mass at T = 0 days. The largest loss of mass was observed between T = 5 and 10 days, increasing from 0.04 ± 0.08% to 0.54 ± 0.45%, while it remained at that level thereafter.

3.4. Mechanical properties of scaffold

Stress-strain graphs are presented in Fig. 6(a) for the entire strain range of the tests for samples at degradation time points T= 0, 10, and 30 days and in Fig. 6(b) for limited to the strain range of the load cycles with upper limit of ε = 20% for degradation time points of T = 0 and 30 days. (The graph for T = 15 days was omitted from Fig. 6b to improve clarity). The maximum stress σ_{max} and associated strain ε_{max} versus degradation time T are illustrated in Fig. 7(a). The stress did not exhibit a change after the first five days of degradation and decreased steadily thereafter. The maximum stress ranged from σ_{max} = 0.52 ± 0.12 MPa at T = 0 days to σ_{max} = 0.033 ± 0.028 MPa after a degradation period of T = 34 days. When compared to T = 0 days, the decrease in σ_{max} was statistically non-significant up to T = 14 days but became statistical significant thereafter. The strain ε_{max} decreased statistically significantly between T = 0 days (ε_{max}= 176.8 ± 21.9%) and T = 14 days (ε_{max}= 46.72 ± 2.35%). After T = 14 days, the decrease of ε_{max} to the minimum of 24.6 ± 3.0% at T = 34 days occurred at a reduced rate and was non-significant.

Figure 7(b) illustrates the stress $\sigma_{20\%,i}$ for each repetitive loading event (i = 1 to 6) at each degradation time point. Generally, the stress $\sigma_{20\%,i}$ decreased with repeated loading. The reduction in stress due to repeated loading (cycling) was less pronounced, and not statistically significant, for the degradation periods up to T = 18 days. During the sixth loading, the stress $\sigma_{20\%,6}$ reached between 92.4 ± 2.1% (at T = 0 days) and 90.6 ± 1.9% (at T = 18 days) of the initial value at the first loading $\sigma_{20\%,1}$, see Fig. 7(c). At degradation of T = 22 days and longer, the reduction of $\sigma_{20\%,i}$ due to repeated loading increased with degradation time and the ratios $\sigma_{20\%,6}/\sigma_{20\%,1}$ became statistically significant at T = 30

and 34 days ($p = 0.00016$ and 0.00014, respectively, when compared to T = 18 days). At T = 34 days, the ratios $\sigma_{20\%,6}/\ \sigma_{20\%,1}$ was at a minimum of 28.5 ± 16.4%.

Figure 8 shows the elastic modulus, $E_{\varepsilon,i}$, plotted against strain ε for the first and sixth loading for all degradation time points T. During the first cycle, the elastic modulus exhibited an initial increase with increasing strain but decreased after reaching a maximum between ε = 4 and 8%, irrespective of the degradation period. However, a steady increase of elastic modulus with increasing strain was typically observed during the sixth loading. Overall, the key values of the elastic modulus for the first loading were $E_{0\%,1} = 0.48 \pm 0.35$ MPa, $E_{8\%,1} = 0.92 \pm 0.22$ MPa and $E_{18\%,1} = 0.67 \pm 0.29$ MPa compared to the values during the sixth loading of $E_{0\%,6} = 0.19 \pm 0.19$ MPa, $E_{8\%,6} = 0.58 \pm 0.35$ MPa and $E_{18\%,6} = 1.1 \pm 0.42$ MPa (all values grand means over all degradation time points). The maximum elastic modulus during the first and sixth loading, $E_{max,1}$ and $E_{max,6}$, respectively, is provided in Table 1 for scaffolds prior to degradation and for different degradation times points T = 5 to 34 days.

4. DISCUSSION

In this study we investigated the changes in tensile mechanical properties of electro-spun biodegradable polyurethane (DegraPol® D30) scaffolds for soft tissue regeneration due to hydrolytic *in vitro* degradation of up to 34 days. The mechanical characterisation by means of uni-axial tensile testing incorporated load cycling between 0 and 20% strain in an attempt to simulate the physiological strain regime, or at least part thereof.

The mechanical properties of the electro-spun DegraPol® scaffold deteriorated dramatically during the degradation period of 34 days. The maximum stress, σ_{max}, did not change significantly during the first 14 days of degradation but decreased steadily thereafter, dropping to 6.4% of the initial value after 34 days. The strain, ε_{max}, associated with the maximum stress displayed a different change: from the start of the degradation it decreased rapidly to 26.4% during the first 14 days and decreased markedly slower thereafter to 13.9% after 34 days. The change in the strain ε_{max} coincided with the specification of the manufacturer that indicates complete degradation of DegraPol® D30 with respect to the mechanical properties within two weeks. With increasing degradation time, the electro-spun

scaffold became more susceptible to load cycling. A reduction of the stress at a strain of 20% with repeated loading was observed in all samples. For degradation times of up to 18 days, the stress reduction was non-significant and resembled a mechanical conditioning which is also observed in other materials such as Nitinol[32] and biological soft tissues.[33] For a degradation time of 22 days and longer, the stress reduction became statistically significant, now governed by the reduced strength of the material. The elastic modulus also decreased with degradation time, the change was however less pronounced as that of the maximum stress and associated strain. The increase of the elastic modulus with increasing strain observed during the 6th loading cycle is typical feature of non-linear stiffening. Such a mechanical behaviour is observed in biological soft tissues such as arteries[34] and may be desirable for implant materials, e.g. biomedical coarse knit fabrics,[15,35] that aim at simulating physiological mechanics. The deterioration of physical properties due to degradation was not reflected in scaffold mass. The mass of the samples remained nearly constant over the entire degradation period.

In order to assess the data of mechanical characteristics of the current study against that reported in literature, scaffold structure and materials used need to be compared. The fibre thickness of the scaffold was found to be similar to electro-spun DegraPol® scaffolds used in previous studies.[14,22] While the amount of fibre alignment appeared to be similar to that of the scaffold by Riboldi et al.[14] from visual inspection of SEM images, the 2D FFT analysis indicated a lower amount of alignment in the direction of rotation in the scaffold used in the current study. It was also found that the fibre alignment was more pronounced on the outer surface than on the inner surface. This can be explained with an increase in tangential velocity on the target surface during the spinning process that is associated with the increase in target diameter due to scaffold build-up, and which has been reported to affect fibre alignment.[31]

The mechanical properties obtained for the non-degraded scaffold were lower compared to electro-spun DegraPol® D15.[14] The maximum stress, associated strain and elastic modulus reported were 4.8-, 1.25- and 6.26-fold (σ_{max} = 2.52±0.17MPa, ε_{max} = 220.40±57.09%, E = 10.15±0.69MPa) of that values obtained in the current study. Since the ratio of hard- and soft segment of the two DegraPol®

variants was identical (personal communications: S. Mantero, Politecnico di Milano, 23/06/2010; E. Bonavoglia, ab medica S.p.A, 28/06/2010), the higher mechanical properties of the scaffold of Riboldi et al.[14] were ascribed to a more pronounced fibre alignment (Supplement Fig. A).[13,31] The scaffold exhibited slightly higher mechanical properties, except for ε_{max}, after 5 days degradation compared to the non-degraded state (see Fig. 7a for σ_{max}, Fig. 7b for $\sigma_{20\%,i}$ and Table 1 for E). The reason for this, although not statistically significant, difference may be the fact that the non-degraded samples were not submerged in water prior to testing. The swelling of fibres during submersion could affect the mesh structure irreversibly.[28]

The elastic modulus of electro-spun DegraPol® has previously been reported as being constant up to 10% strain.[14] Although a constant elastic modulus - be it in bulk or processed form of the material - gives an indication of the material stiffness,[14,21,22] more in depth information is beneficial for constitutive modelling and computational mechanics. The analysis carried out in the current study indicated a variation of the elastic modulus both with the change in magnitude of strain and the number of loadings. For the initial loading, the elastic modulus was found to increase on average by 91% with the strain increasing from 0% to 8% while it decreased from this maximum value by 27% with the strain further increasing to 18%. A different characteristic was observed during the final loading with the elastic modulus steadily increasing by 501% with the strain increasing from 0% to 18%. This pattern was found for the non-degraded scaffold as well as for all degradation time points. Similar changes of the elastic modulus with strain and effects of load cycling were reported for electro-spun polycaprolactone (PCL) for a strain up to 35%.[24]

The lack of mass loss indicated that the degradation occurred on a molecular level only but did not progress far enough to cause a significant volume of fibres to dissolve or break off. This is supported by the SEM micrographs which did not show significant fibre surface changes between samples after 34 days degradation and non-degraded samples. Lendlein et al.[21] and Riboldi et al.[14] reported a reduction in molecular mass immediately after the start of the degradation. However, a reduction in sample mass has been reported to commence only between 28 and more than 100 days after degradation onset depending on the specific DegraPol® version tested.[21] The reduction in molecular

mass without loss in scaffold mass in the early stages of degradation has been reported to be caused by random hydrolytic cleavage of the macromolecular chains. The loss of sample mass commenced once the molecular mass dropped below a certain threshold at which polymer segments became small enough to filter out of the bulk polymer.[21] Furthermore, significant changes in mechanical strength were reported in the same time period as molecular mass changes.[14,21,28] This indicates that a change in mass, or lack thereof, of a sample is not an appropriate measure of the degree of degradation with respect to mechanical properties. It is however important to investigate the loss in sample mass, and material volume, as an indication of space available for ingrowth of cells and tissue.

During tensile testing of the scaffolds after longer degradation times, it was found that some samples exhibited severe plastic deformation (see Fig. 4 b, d), disintegration and, in some instances, failure during one of the load cycles, i.e. prior to the final loading. For future studies, a decrease of the upper strain limit of $\varepsilon = 20\%$ for the load cycles may be considered to prevent excessive plastic deformation during cycling and to determine the change of the elastic limit of the scaffold with progressing degradation. When evaluating the increasing lack of structural stability of the degrading scaffold, the potential mechanical effect of tissue regenerating in the scaffold needs to be considered. For the design of a tissue regenerating implant, the structural degradation of the scaffold needs to be adjusted to the rate of tissue regeneration so as to prevent structural failure of the implant. If this is not feasible, alternatives designs need to ensure structural integrity of the implant, for example composite structures comprising two or more components.

Apart from the limited amount of research on the mechanical characterisation of biodegradable electro-spun scaffolds in literature, the comparison of the results of the current study with previous work was also intricate due to differences in materials and study parameter e.g. of the scaffold manufacturing. Despite the similar approach of preparation of scaffolds and samples, a dissimilar target shape for the electro-spinning of the current study and those used by Ayres et al.[31] may have contributed to the difference in mechanical properties observed.

This study is a first step to extend the research in mechanics and constitutive modelling of degrading tissue regenerative scaffolds. Future studies with extensions of the work presented, e.g. use of

physiological degradation solution such as phosphate buffered saline, characterisation of molecular weight of the scaffold, and changes thereof during degradation, will provide important additional data. With the aim of developing comprehensive constitutive models for scaffold-based soft tissue regeneration, further research will also address important aspects such as strain rate sensitivity of the scaffold material, effect of tissue incorporation and application-specific mechanics.

CONCLUSIONS

The mechanical characterisation of rapidly degrading polymeric porous scaffolds for tissue regenerative application is important to prevent the failure of such implants due to the loss of structural integrity before regenerated tissue can provide sufficient mechanical support. These time-dependent processes need to be considered during the development of tissue regenerative implants. The results of the current study are a first step in the characterisation of the effects of biodegradation on the mechanical properties of such scaffolds. They can provide a basis for the development of constitutive models of biodegradable scaffolds and the extension to capture mechanical effects of regenerating tissue.

ACKNOWLEDGEMENTS

The authors thank ab medica S.p.A for donating the DegraPol® material for this study. ETH Zurich and University of Zurich are owners and ab medica S.p.A is exclusive licensee of all IP Rights of DegraPol®.

FUNDING SOURCES

This study was supported financially by the National Research Foundation (NRF) of South Africa. Any opinion, findings and conclusions or recommendations expressed in this publication are those of the authors and therefore the NRF does not accept any liability in regard thereto.

CONFLICT OF INTEREST STATEMENT

The authors declare that they do not have conflicts of interest with regard to this manuscript and the data presented therein.

REFERENCES

1. Furth ME, Atala A, Van Dyke ME. Smart biomaterials design for tissue engineering and regenerative medicine. Biomaterials 2007;28:5068-5073.

2. Williams DF. To engineer is to create: the link between engineering and regeneration. Trends in Biotechnology 2006;24:4-8.

3. Zilla P, Bezuidenhout D, Human P. Prosthetic vascular grafts: Wrong models, wrong questions and no healing. Biomaterials 2007;28:5009-5027.

4. Kang Y, Yao Y, Yin G, Huang Z, Liao X, Xu X, Zhao G. A study on the in vitro degradation properties of poly(l-lactic acid)/[beta]-tricalcuim phosphate(PLLA/[beta]-TCP) scaffold under dynamic loading. Medical Engineering & Physics 2009;31:589-594.

5. Keskar V, Gandhi M, Gemeinhart EJ, Gemeinhart RA. Initial evaluation of vascular ingrowth into superporous hydrogels. Journal of Tissue Engineering and Regenerative Medicine 2009;3:486-490.

6. Bezuidenhout D, Davies N, Zilla P. Effect of well defined dodecahedral porosity on inflammation and angiogenesis. Asaio J 2002;48:465-71.

7. Davies N, Dobner S, Bezuidenhout D, Schmidt C, Beck M, Zisch AH, Zilla P. The dosage dependence of VEGF stimulation on scaffold neovascularisation. Biomaterials 2008;29:3531-3538.

8. Hou Q, Grijpma DW, Feijen J. Porous polymeric structures for tissue engineering prepared by a coagulation, compression moulding and salt leaching technique. Biomaterials 2003;24:1937-1947.

9. Yoon JJ, Park TG. Degradation behaviors of biodegradable macroporous scaffolds prepared by gas foaming of effervescent salts. Journal of Biomedical Materials Research 2001;55:401-408.

10. Sarkar S, Burriesci G, Wojcik A, Aresti N, Hamilton G, Seifalian AM. Manufacture of small calibre quadruple lamina vascular bypass grafts using a novel automated extrusion-phase-inversion method and nanocomposite polymer. Journal of Biomechanics 2009;42:722-730.

11. Guan J, Fujimoto KL, Sacks MS, Wagner WR. Preparation and characterization of highly porous, biodegradable polyurethane scaffolds for soft tissue applications. Biomaterials 2005;26:3961-71.

12. McClure MJ, Sell SA, Simpson DG, Walpoth BH, Bowlin GL. A three-layered electrospun matrix to mimic native arterial architecture using polycaprolactone, elastin, and collagen: A preliminary study. Acta Biomaterialia 2010;In Press, Corrected Proof.

13. Ayres CE, Bowlin GL, Henderson SC, Taylor L, Shultz J, Alexander J, Telemeco TA, Simpson DG. Modulation of anisotropy in electrospun tissue-engineering scaffolds: Analysis of fiber alignment by the fast Fourier transform. Biomaterials 2006;27:5524-5534.

14. Riboldi SA, Sampaolesi M, Neuenschwander P, Cossu G, Mantero S. Electrospun degradable polyesterurethane membranes: potential scaffolds for skeletal muscle tissue engineering. Biomaterials 2005;26:4606-15.

15. Yeoman MS, Reddy BD, Bowles H, Zilla P, Bezuidenhout D, Franz T. The Use of Finite Element Methods and Genetic Algorithms in Search of an Optimal Fabric Reinforced Porous Graft System. Annals of Biomedical Engineering 2009;37:2266-2287.

16. Zidi M, Cheref M. Mechanical analysis of a prototype of small diameter vascular prosthesis: numerical simulations. Comput Biol Med 2003;33:65-75.

17. Sill TJ, von Recum HA. Electrospinning: Applications in drug delivery and tissue engineering. Biomaterials 2008;29:1989-2006.

18. Hollister SJ, Lin CY. Computational design of tissue engineering scaffolds. Computer Methods in Applied Mechanics and Engineering 2007;196:2991-2998.

19. Di Prima M, Gall K, McDowell DL, Guldberg R, Lin A, Sanderson T, Campbell D, Arzberger SC. Deformation of epoxy shape memory polymer foam. Part I: Experiments and macroscale constitutive modeling. Mechanics of Materials 2010;42:304-314.

20. He HB, Matsuda T. Arterial replacement with compliant hierarchic hybrid vascular graft: Biomechanical adaptation and failure. Tissue Engineering 2002;8:213-224.

21. Lendlein A, Colussi M, Neuenschwander P, Suter UW. Hydrolytic Degradation of Phase-Segregated Multiblock Copoly(ester urethane)s Containing Weak Links. Macromolecular Chemistry and Physics 2001;202:2702-2711.

22. Lendlein A, Neuenschwander P, Suter UW. Tissue-compatible multiblock copolymers for medical applications, controllable in degradation rate and mechanical properties. Macromolecular Chemistry and Physics 1998;199:2785-2796.

23. Kwon IK, Kidoaki S, Matsuda T. Electrospun nano- to microfiber fabrics made of biodegradable copolyesters: structural characteristics, mechanical properties and cell adhesion potential. Biomaterials 2005;26:3929-3939.

24. Duling RR, Dupaix RB, Katsube N, Lannutti J. Mechanical Characterization of Electrospun Polycaprolactone (PCL): A Potential Scaffold for Tissue Engineering. Journal of Biomechanical Engineering 2008;130:011006-13.

25. Lee SJ, Liu J, Oh SH, Soker S, Atala A, Yoo JJ. Development of a composite vascular scaffolding system that withstands physiological vascular conditions. Biomaterials 2008;29:2891-2898.

26. Vaz CM, van Tuijl S, Bouten CVC, Baaijens FPT. Design of scaffolds for blood vessel tissue engineering using a multi-layering electrospinning technique. Acta Biomaterialia 2005;1:575-582.

27. Mirensky TL, Fein CW, Nguyen GK, Hibino N, Sawh-Martinez RF, Yi T, McGillicuddy EA, Villalona G, Shinoka T, Breuer CK. Characterization of small-diameter electrospun tissue-engineered arterial grafts. Journal of the American College of Surgeons 2009;209:S30-S30.

28. Henry JA, Simonet M, Pandit A, Neuenschwander P. Characterization of a slowly degrading biodegradable polyesterurethane for tissue engineering scaffolds. Journal of Biomedical Materials Research Part A 2007;82A:669-679.

29. Milleret V, Simonet M, Bittermann AG, Neuenschwander P, Hall H. Cyto- and hemocompatibility of a biodegradable 3D-scaffold material designed for medical applications. J Biomed Mater Res B Appl Biomater 2009;91:109-21.

30. Ayres CE, Jha BS, Meredith H, Bowman JR, Bowlin GL, Henderson SC, Simpson DG. Measuring fiber alignment in electrospun scaffolds: a user's guide to the 2D fast Fourier transform approach. Journal of Biomaterials Science, Polymer Edition 2008;19:603-621.

31. Ayres CE, Bowlin GL, Pizinger R, Taylor LT, Keen CA, Simpson DG. Incremental changes in anisotropy induce incremental changes in the material properties of electrospun scaffolds. Acta Biomaterialia 2007;3:651-661.

32. van der Merwe H, Reddy BD, Zilla P, Bezuidenhout D, Franz T. A computational study of knitted Nitinol meshes for their prospective use as external vein reinforcement. Journal of Biomechanics 2008;41:1302-1309.

33. Carew EO, Barber JE, Vesely I. Role of preconditioning and recovery time in repeated testing of aortic valve tissues: validation through quasilinear viscoelastic theory. Ann Biomed Eng 2000;28:1093-100.

34. Valdez-Jasso D, Bia D, Zócalo Y, Armentano R, Haider M, Olufsen M. Linear and Nonlinear Viscoelastic Modeling of Aorta and Carotid Pressure–Area Dynamics Under <i>In

Vivo</i> and <i>Ex Vivo</i> Conditions. Annals of Biomedical Engineering 2011:1-19.

35. Yeoman MS, Reddy D, Bowles HC, Bezuidenhout D, Zilla P, Franz T. A constitutive model for the warp-weft coupled non-linear behavior of knitted biomedical textiles. Biomaterials 2010;31:8484-8493.

TABLES

Table 1. Maximum elastic modulus (mean ± stdev) of the electro-spun scaffold at the first loading ($E_{max,1}$) and sixth loading ($E_{max,6}$) prior to degradation (T = 0 days) and after different times of degradation (T = 5 to 34 days).

T (days)	**$E_{max,1}$ (MPa)**	**$E_{max,6}$ (MPa)**
0	0.99 ± 0.16	1.14 ± 0.23
5	1.29 ± 0.35	1.64 ± 0.56
10	1.23 ± 0.16	1.54 ± 0.17
14	0.98 ± 0.09	1.21 ± 0.20
18	0.99 ± 0.12	1.19 ± 0.13
22	1.03 ± 0.14	1.30 ± 0.05
26	0.99 ± 0.34	1.15 ± 0.41
30	0.95 ± 0.20	0.82 ± 0.13
34	0.76 ± 0.10	0.43 ± 0.26
All Grps	1.02 ± 0.24	1.17 ± 0.42

FIGURES

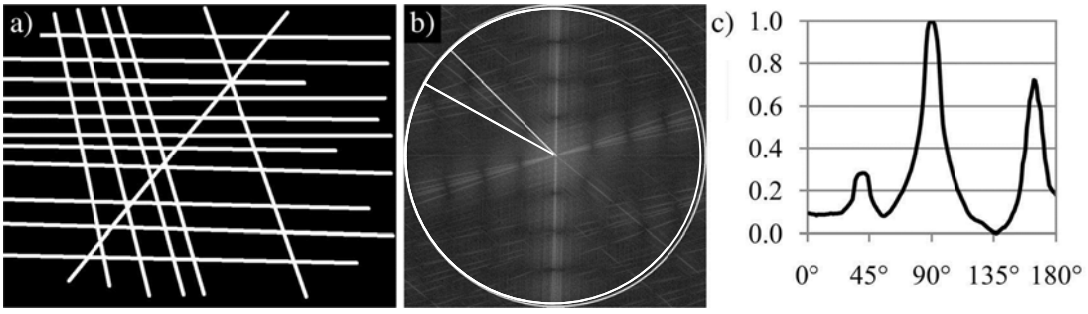

Figure 1. Example of alignment measure a) Example of fibre pattern with predominant alignment in one direction; b) FFT power spectrum of example fibre pattern (a) showing perimeter of circular summation field and one radial summation line; c) Normalised amount of fibre alignment of example fibre pattern

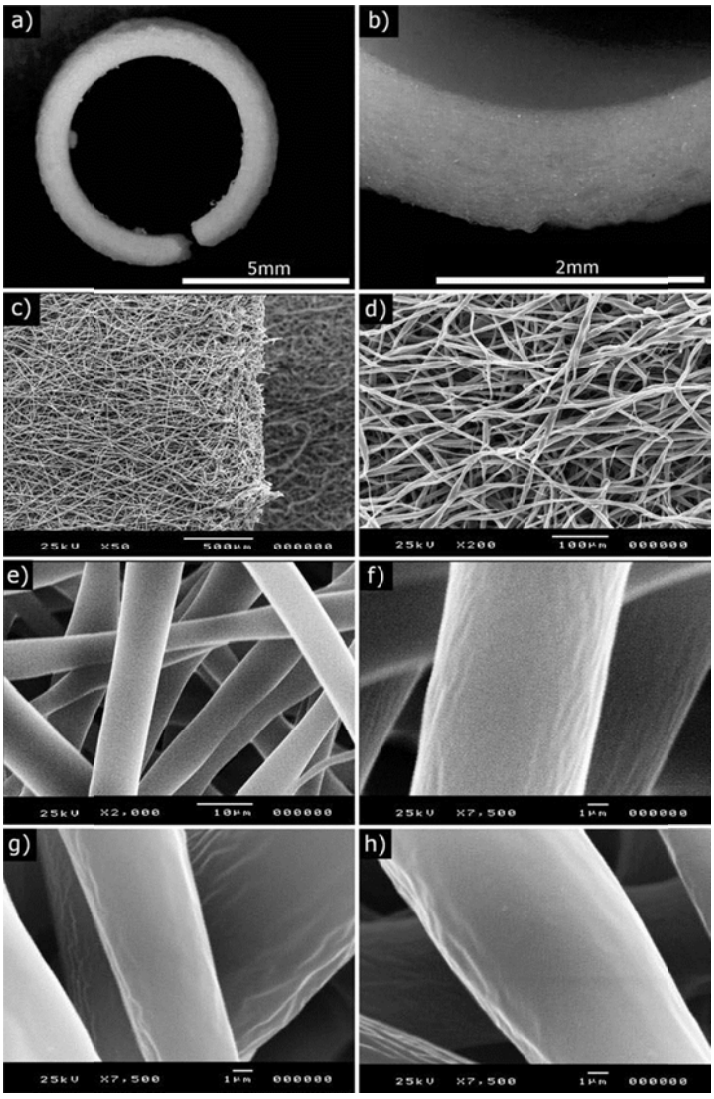

Figure 2: Gross photographs and micrographs of non-degraded (a-f) and partially degraded (g, h) electro-spun scaffold samples. The magnification and scale bar length are provided in parenthesis for each micrograph. a) Low magnification cross-sectional view of sample with longitudinal cut (x1, 5 mm); b) View of portion of cross-section used for measurement of the wall thickness (x4, 2 mm); c) Outside surface of scaffold (left portion of image) with cut edge. (x50, 500 µm); d) View of inner surface used for analysis of fibre alignment (x200, 100 µm); e) High magnification image used for measurement of fibre thickness (x2000, 10 µm); f) Section of single fibre of non-degraded sample (x7500, 1 µm); g) Section of fibre after 14 days of degradation (x7500, 1 µm); h) Section of fibre after 34 days of degradation (x7500, 1 µm). There was no change of the fibre surface between degraded and non-degraded samples.

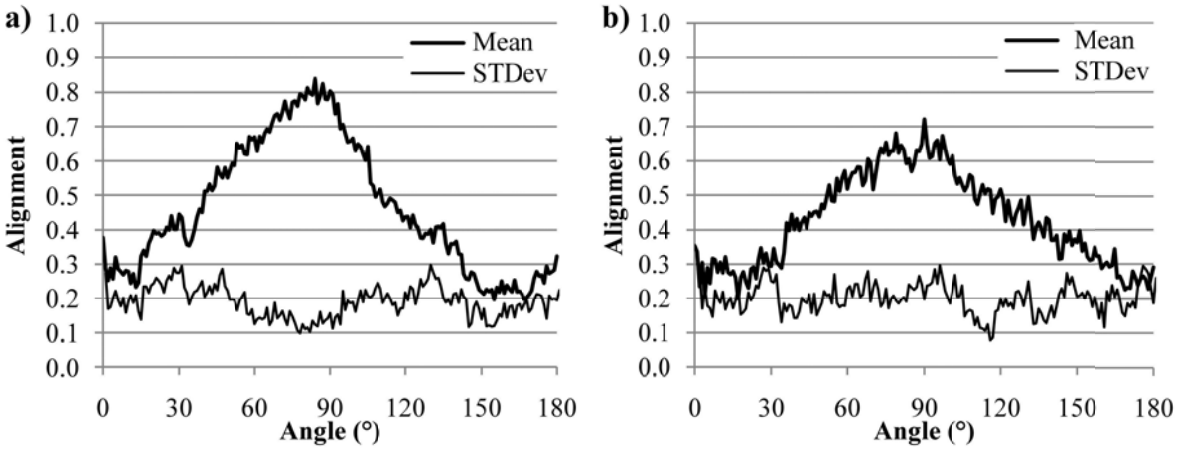

Figure 3: Normalised amount of fibre alignment on the outer surface (a) and inner surface (b) of the electro-spun scaffolds versus analysis angle. The analysis angles of 0° and 180° coincide with the longitudinal axis of the target mandrel, and electro-spun tube, whereas the angle of 90° refers to the circumferential direction.

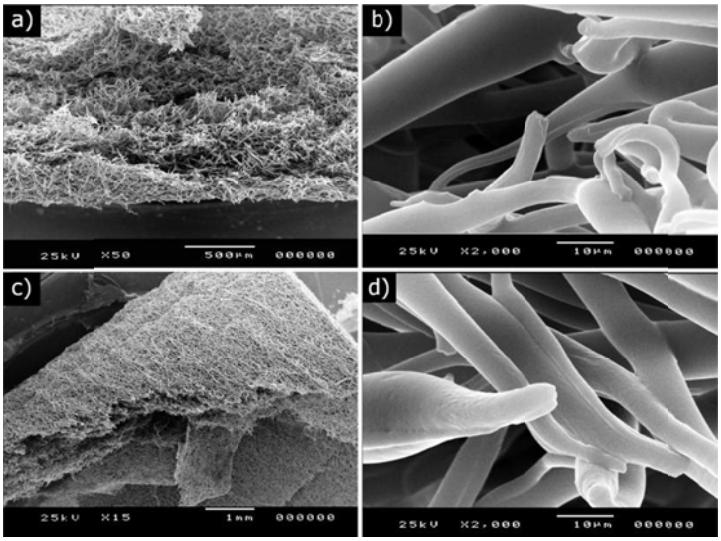

Figure 4: Scanning electron micrographs of scaffold samples after mechanical testing to failure following degradation for 5 days (a: x50, 500 µm; b: x2000, 10 µm) and 26 days (c: x15, 1 mm; d: x2000, 10 µm). The magnification and scale bar length are provided in parenthesis.

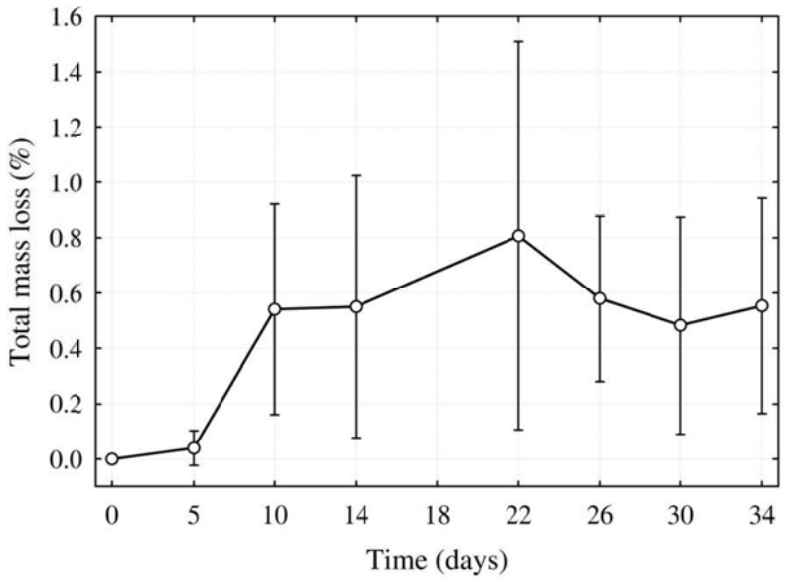

Figure 5: Cumulative loss of mass, as a percentage of the original sample mass at T = 0 days, versus the degradation time.

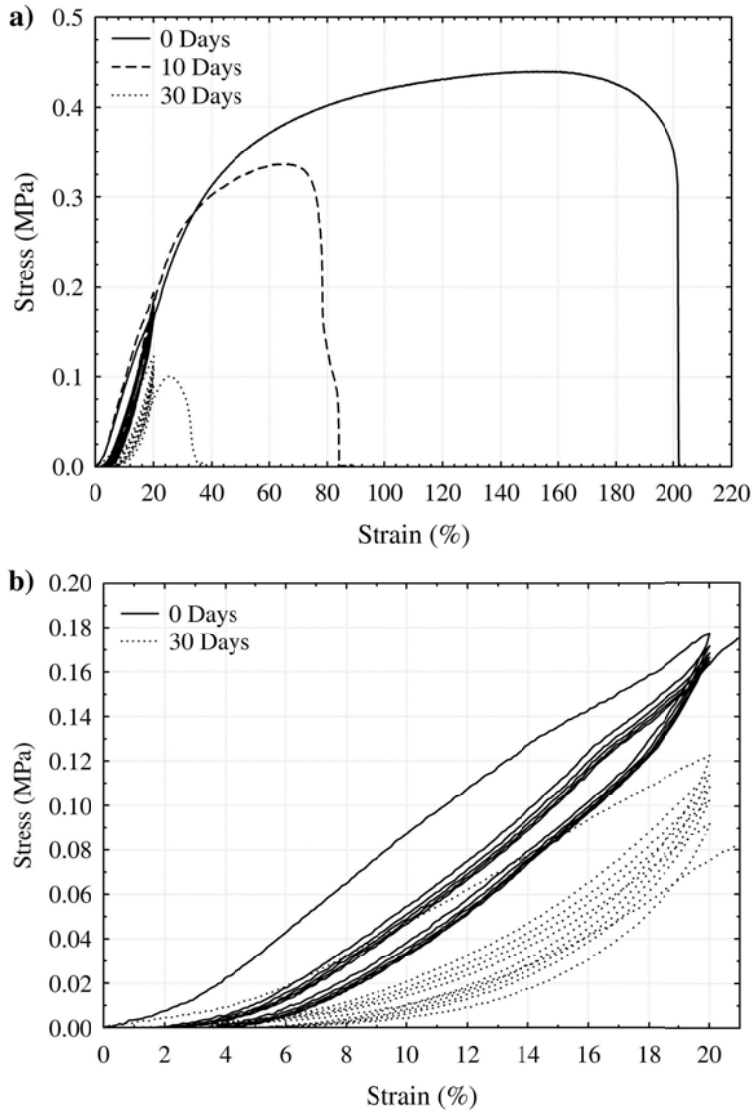

Figure 6: Graphs of tensile stress, σ, versus tensile strain, ε, representing a) Five initial loading-unloading cycles and final loading until failure of non-degraded sample (T = 0 days) and samples degraded for 15 and 30 days, respectively (T = 10, 30 days) and b) Close-up of five initial load cycles of non-degraded sample (T = 0 days) and samples degraded for 30 days (T = 30 days), showing decrease of stress at upper limit of cyclic strain of 20% with increasing number of cycles. The graph for the sample with T = 10 days degradation was omitted to improve clarity of the illustration.

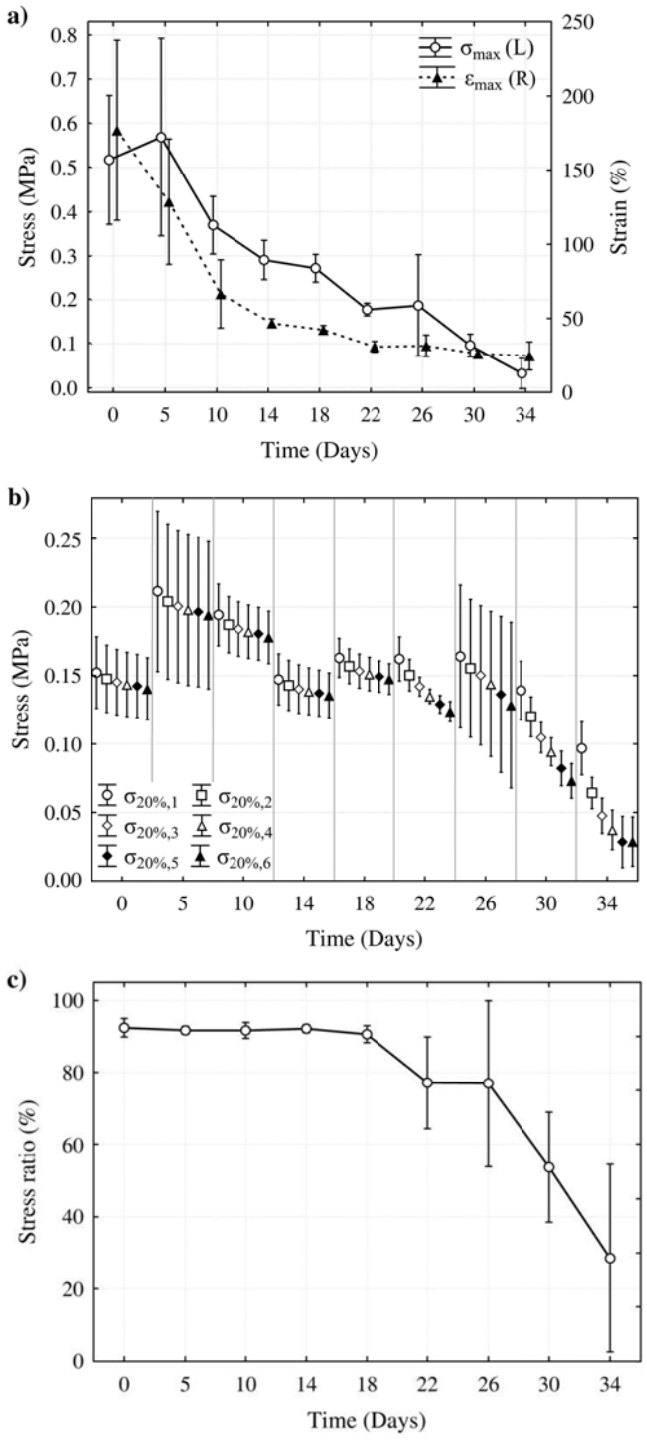

Figure 7: Characteristic stress and strain data versus degradation time in non-degraded samples (T = 0 days) and degraded samples (T = 5 – 34 days): a) Maximum stress, σ_{max}, and corresponding strain, ε_{max}, versus degradation time; b) Stress $\sigma_{20\%,i}$ of the five initial loading cycles (i = 1 to 5) and the final loading (i = 6) versus degradation time; c) Ratio of stress at 20% strain of final loading to stress at 20% strain of first cycle, $\sigma_{20\%,6} / \sigma_{20\%,1}$, versus degradation time.

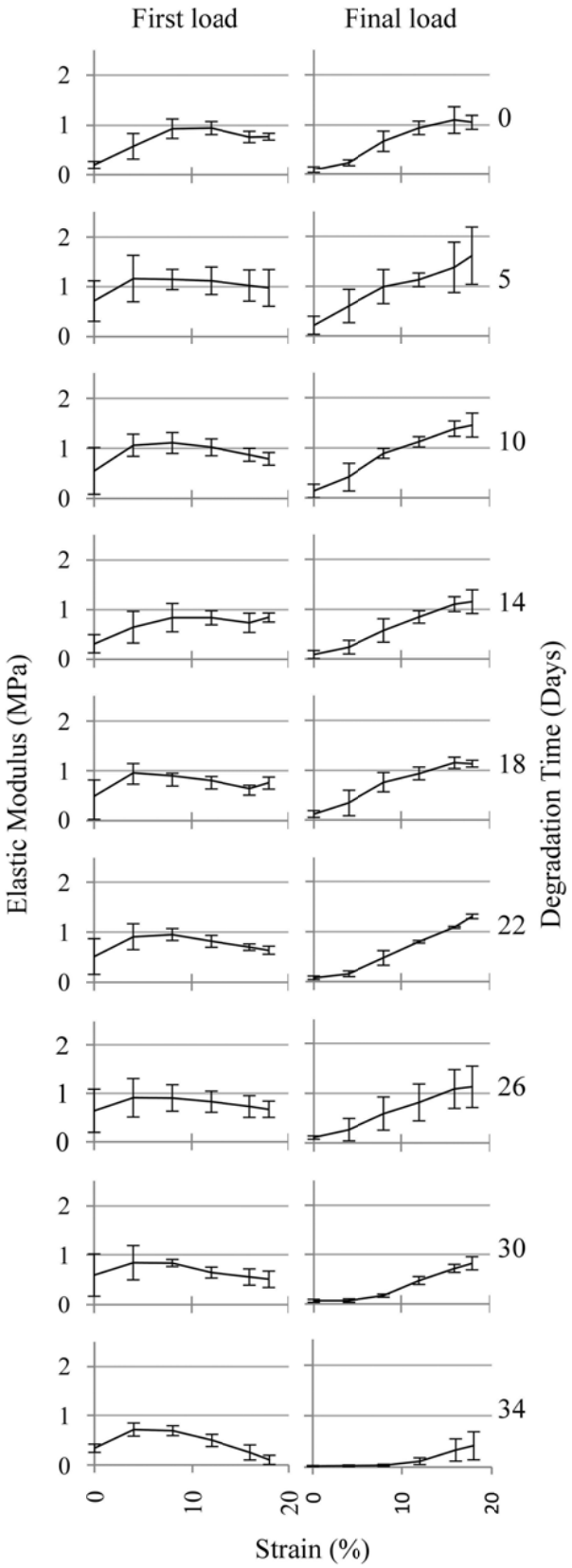

Figure 8: Elastic modulus of the scaffold versus strain during the first loading ($E_{\varepsilon,1}$) and the final loading ($E_{\varepsilon,6}$) at various degradation time points.

SUPPLEMENTS

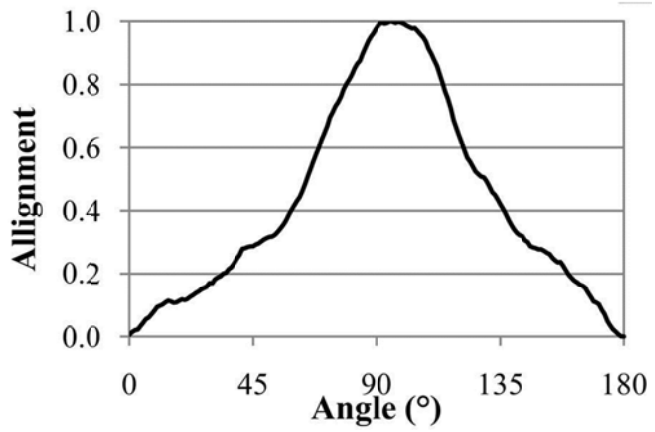

Figure A: Normalised amount of fibre alignment versus analysis angle for an electro-spun scaffold (outside surface) of Riboldi et al. determined with 2D FTT analysis of a published SEM micrograph [14; Fig. 1a]. The analysis angles of 0° and 180° coincide with the longitudinal axis of the target mandrel, and electro-spun tube, whereas the angle of 90° refers to the circumferential direction. The distinguishing characteristic between the alignment distribution of Riboldi et al. compared to the current study is a increased concentration of alignment in spinning direction (90°) and absence of alignment in perpendicular direction (0, 180°).